applied sciences

MDPI

Article

Artificial Intelligence Applications on Restaging [^{18}F]FDG PET/CT in Metastatic Colorectal Cancer: A Preliminary Report of Morpho-Functional Radiomics Classification for Prediction of Disease Outcome

Pierpaolo Alongi [1,2], Alessandro Stefano [3], Albert Comelli [4,*], Alessandro Spataro [5], Giuseppe Formica [5], Riccardo Laudicella [1,4,5,6], Helena Lanzafame [5], Francesco Panasiti [5], Costanza Longo [5], Federico Midiri [7], Viviana Benfante [4,8], Ludovico La Grutta [8], Irene Andrea Burger [6,9], Tommaso Vincenzo Bartolotta [7], Sergio Baldari [5], Roberto Lagalla [7], Massimo Midiri [7] and Giorgio Russo [3]

1 Nuclear Medicine Unit, Fondazione Istituto Giuseppe Giglio, 90015 Cefalù, Italy; alongi.pierpaolo@gmail.com (P.A.); riccardo.laudicella@usz.ch (R.L.)
2 Nuclear Medicine Unit, A.R.N.A.S. Ospedale Civico Di Cristina e Benfratelli, 90127 Palermo, Italy
3 Institute of Molecular Bioimaging and Physiology, National Research Council (IBFM-CNR), 90015 Cefalù, Italy; alessandro.stefano@ibfm.cnr.it (A.S.); giorgio.russo@ibfm.cnr.it (G.R.)
4 Ri.MED Foundation, 90133 Palermo, Italy; vbenfante@Fondazionerimed.com
5 Nuclear Medicine Unit, Department of Biomedical and Dental Sciences and Morpho-Functional Imaging, University of Messina, 98122 Messina, Italy; alessandro.spataro@outlook.it (A.S.); giuseppeformica23@gmail.com (G.F.); helena.lanzafame@gmail.com (H.L.); francesco.panasiti90@gmail.com (F.P.); costanza.longo@virgilio.it (C.L.); sbaldari@unime.it (S.B.)
6 Department of Nuclear Medicine, University Hospital Zurich, University of Zurich, 8091 Zurich, Switzerland; Irene.burger@usz.ch
7 Section of Radiological Sciences, Department of Biomedicine, Neuroscience and Advanced Diagnostics, University of Palermo, 90133 Palermo, Italy; federico.midiri@hotmail.com (F.M.); tommasovincenzo.bartolotta@unipa.it (T.V.B.); roberto.lagalla@unipa.it (R.L.); massimo.midiri@unipa.it (M.M.)
8 Department of Health Promotion, Mother and Child Care, Internal Medicine and Medical Specialties, Molecular and Clinical Medicine, University of Palermo, 90127 Palermo, Italy; ludovico.lagrutta@unipa.it
9 Department of Nuclear Medicine, Kantonsspital Baden, 5404 Baden, Switzerland
* Correspondence: acomelli@fondazionerimed.com

check for updates

Citation: Alongi, P.; Stefano, A.; Comelli, A.; Spataro, A.; Formica, G.; Laudicella, R.; Lanzafame, H.; Panasiti, F.; Longo, C.; Midiri, F.; et al. Artificial Intelligence Applications on Restaging [^{18}F]FDG PET/CT in Metastatic Colorectal Cancer: A Preliminary Report of Morpho-Functional Radiomics Classification for Prediction of Disease Outcome. *Appl. Sci.* **2022**, *12*, 2941. https://doi.org/10.3390/app12062941

Academic Editor: Qi-Huang Zheng

Received: 17 February 2022
Accepted: 9 March 2022
Published: 13 March 2022

Publisher's Note: MDPI stays neutral with regard to jurisdictional claims in published maps and institutional affiliations.

Featured Application: Based on results defined in this study, new investigations might propose morpho-functional-based radiomics algorithms for risk stratification with possible impact on treatment management in colorectal cancer.

Abstract: The aim of this study was to investigate the application of [^{18}F]FDG PET/CT images-based textural features analysis to propose radiomics models able to early predict disease progression (PD) and survival outcome in metastatic colorectal cancer (MCC) patients after first adjuvant therapy. For this purpose, 52 MCC patients who underwent [^{18}F]FDGPET/CT during the disease restaging process after the first adjuvant therapy were analyzed. Follow-up data were recorded for a minimum of 12 months after PET/CT. Radiomics features from each avid lesion in PET and low-dose CT images were extracted. A hybrid descriptive-inferential method and the discriminant analysis (DA) were used for feature selection and for predictive model implementation, respectively. The performance of the features in predicting PD was performed for per-lesion analysis, per-patient analysis, and liver lesions analysis. All lesions were again considered to assess the diagnostic performance of the features in discriminating liver lesions. In predicting PD in the whole group of patients, on PET features radiomics analysis, among per-lesion analysis, only the GLZLM_GLNU feature was selected, while three features were selected from PET/CT images data set. The same features resulted more accurately by associating CT features with PET features (AUROC 65.22%). In per-patient analysis, three features for stand-alone PET images and one feature (i.e., HUKurtosis) for the PET/CT data set were selected. Focusing on liver metastasis, in per-lesion analysis, the same analysis recognized one PET feature (GLZLM_GLNU) from PET images and three features from PET/CT data set. Similarly,

in liver lesions per-patient analysis, we found three PET features and a PET/CT feature (HUKurtosis). In discrimination of liver metastasis from the rest of the other lesions, optimal results of stand-alone PET imaging were found for one feature (SUVbwmin; AUROC 88.91%) and two features for merged PET/CT features analysis (AUROC 95.33%). In conclusion, our machine learning model on restaging [^{18}F]FDGPET/CT was demonstrated to be feasible and potentially useful in the predictive evaluation of disease progression in MCC.

Keywords: colon; cancer; radiomics; artificial intelligence; positron emission tomography-computed tomography; nuclear medicine

1. Introduction

Colorectal cancer (CRC) is the third most common cancer and the second leading cause of death worldwide. Almost 20% of such patients will develop metastatic disease, about one-third of patients already present with liver metastases at the time of diagnosis [1,2]. Alongside traditional imaging (e.g., ultrasonography, CT, MRI), [^{18}F]FDG PET/CT is routinely used as a tool for accurate staging and restaging after therapy in patients with colorectal metastatic disease, and it represents a valuable ally for risk assessment, prognosis evaluation, and treatment strategy decisions making.

Radiomics is that part of artificial intelligence (AI) that aims to provide quantitative characteristics (features) from biomedical images of different nature that cannot be assessed by the human eye, assuming that any smallest image's constituent (i.e., voxel and/or pixel) may encompass features of tumor's phenotypes that may be potentially related to tumor's outcome and patients' response to therapy, reflecting the pathophysiological process and supporting medical decisions. The workflow of radiomics' processes can be simply resumed in five main steps starting with the acquisition of images, pre-processing tasks (registration, deconvolution, denoizing, and so on) and VOI delineation, features extraction, reduction, and selection, and finally, the selection of the predictive model using AI-based classifiers [3]. In the last decade, the use of radiomics in the study of medical images has aroused increasing interest [4,5]. Several studies have demonstrated the correlation between the heterogeneity of the tissues and the radiomics features, which would allow obtaining relevant information through the analysis of the images alone [6].

[^{18}F]FDG PET/CT could be a useful modality for assessing tumor viability and differential diagnosis also for colorectal metastatic cancer and may provide important data regarding the appropriate treatment strategy [7,8]. The further integration of [^{18}F]FDG PET/CT data with radiomics features could reach the provision of new insightful information also regarding tumor biology. In other words, the statistical analysis of the features using methods of increasing complexity (first order, second order, or higher) can be useful in the prognostic evaluation, in therapeutic management, and in characterizing tumor phenotypes [9]. Radiomics' literature in colorectal cancer is highly limited in PET imaging, but it nonetheless holds promise for genetic mutation status assessment [10,11] and the prediction of outcomes.

The present study aimed to investigate the potential application of texture analysis on restaging [^{18}F]FDG PET/CT images in metastatic colorectal patients, proposing a radiomics model able to select PET and CT imaging features for global disease status prediction, liver metastasis evaluation, and survival outcomes.

2. Materials and Methods

Sixty-three metastatic lesions from fifty-two colorectal patients were retrospectively considered. Patients underwent restaging [^{18}F]FDG PET/CT after first adjuvant therapy between November 2008 and December 2018 following these inclusion criteria: (a) pathology confirmed diagnosis of primary colorectal adenocarcinoma; (b) clinical-instrumental (ceCT, MR, histopathology, and/or clinical report) confirmed metastatic disease status;

(c) [^{18}F]FDG PET/CT performed at restaging after first adjuvant therapy (at least 15 days from the last cycle of chemotherapy and three months after RT); (d) [^{18}F]FDG PET/CT positive for lymph-nodal/metastatic disease; (e) minimum follow-up (FU) duration of 12 months after [^{18}F]FDG PET/CT; (f) complete clinical (clinical case notes and multidisciplinary meeting reports), laboratory, pathological and imaging data available (contrast-enhanced CT, MRI); (g) [^{18}F]FDG PET/CT findings retrospectively confirmed at clinical follow-up with biopsy and/or through other imaging modalities. The study was approved by the institutional review board. The internal procedures provide informed consent also regarding the potential scientific use of all nuclear medicine examinations performed at the Fondazione Istituto G.Giglio of Cefalù (Palermo, Italy). Therefore, written informed consent was available for each patient.

2.1. [^{18}F]FDG PET/CT Imaging

According to the standard [^{18}F]FDG PET/CT protocol in use at our institution, the scans were performed following the international clinical recommendations [12]. After six hours of fasting, patients underwent examination on Discovery STE GE Healthcare. The clinical protocol included a full-body PET scan (6–8 beds, 2–3 min per bed position) after 60 min the i.v. administration of 3.7 MBq/kg of [^{18}F]FDG and a co-registered low-dose CT scan (120 kV, 80–120 mA) without contrast enhancement. PET images (256 $\times$ 256 voxel size) were reconstructed with CT-based attenuation correction. The 3D reconstruction was based on the ordered subset expectation maximization (OSEM) algorithm with the two iterative processes. Two nuclear medicine physicians (over 5 years' experience, PA and RL) qualitatively analyze the examinations, being aware of the results of other imaging modalities and clinical data. Following inclusion criteria, [^{18}F]FDG PET/CT positivity was confirmed by the raters after consensus reading if a non-physiological [^{18}F]FDG uptake was moderately (tracer uptake superior to the background at visual assessment) or markedly (tracer uptake superior to physiological liver uptake at visual assessment) increased to the background activity; in case of multiple [^{18}F]FDG uptake foci, the higher qualitative assessed uptake was selected among multiple lesions for each disease location (N and/or M). CT imaging was used to assist the physician in delineating the tumor for local recurrence or lymph node/metastatic disease. Following clinical, laboratory, and CT, MRI, [^{18}F]FDG PET/CT data were recorded. According to such information, the terms disease progression (PD) and stable disease (SD) were used to define the disease status during the follow-up.

2.2. Radiomics Analysis

The volumetric segmentations were performed with the freely available texture analysis LIFEx platform [13] that is the most widely used IBSI (Image Biomarker Standardization Initiative) compliant software in PET imaging to obtain reproducible and robust radiomics features. Specifically, two board-certified nuclear physicians evaluated and segmented PET/CT lesions by consensus and blinded to the purpose of the study and to the pathology information. Signal intensity on PET images was judged as hyperintense when the signal intensity of the tumor was higher than the signal intensity of non-tumoral tissue. SUV_{max} was used as a PET parameter to select the most avid lesion for the global evaluation of disease status and for the most avid liver lesion in every patient. The same volume was transposed in the same region on CT images for extraction of morphological features. Successively, 105 and 66 features were automatically extracted using LifeX starting from the above-mentioned volumes of interest (VOI) from each lesion in PET and CT images, respectively. The extracted features were classified into two categories based on their information type: (I) shape features, which consider the geometric aspects of the VOI, such as shape and volume, (II) statistical features including first-order statistic (histogram-based) features describing intensity values within the target and higher-order statistics (texture) features that are designed to quantify the perceived texture of an image and to provide spatial information of intensities in a VOI. In the last case, five texture classes were considered:

(i) gray-level cooccurrence matrix (GLCM), (ii) gray-level run-length matrix (GLRLM), (iii) gray-level dependence matrix (GLDM), (iv) gray-level zone length matrix (GLZLM), and (v) neigh-boring gray-level dependence matrix (NGLDM). Specifically, (i) GLCM evaluates the incidence of voxels with the same intensities at a predetermined distance along a fixed direction; (ii) GLRLM assesses consecutive voxels with the same intensity along fixed directions; (iii) GLDM counts the number of voxel segments having the same intensity in a given direction; (iv) GLZLM is defined as the number of connected voxels that have equal gray-level intensity; (v) NGTDM assesses the spatial interrelationships between 3 or more voxels [14]. In the work of [13], there is an extensive description of each extracted feature. Successively, the mixed descriptive-inferential sequential approach, as described in two complementary studies [15,16], was used to identify a small set of radiomics features with valuable association with patients' outcomes for better predictive performance, leading to the exclusion of non-reproducible, redundant, and nonrelevant features from the initial feature data set.

After the selection and reduction process, the predictive model was implemented using the discriminant analysis (DA) [17]. The training step was performed only once, and when completed, the DA was capable of classifying new PET lesions. Using the k-fold cross-validation strategy, data were divided into training and validation sets using a random partition. Specifically, data were divided into k-folds: one-fold was used as the validation set while the others folds were used as the training set. The folds were created in such a way that the training and validation sets maintained the same percentage of patient status as the original data set. After applying the trial-and-error methodology, k = 5 was determined as the best value for our analyses (k range: 5–15, step size of 5). Consequently, this process was repeated 5 times, and the mean error was calculated (i) to avoid the over-fitting and asymmetrical sampling by increasing the accuracy of the final results, (ii) to test different models, and (iii) to obtain more robust results [18–22].

The steps between the reduction and selection of features and the implementation of the model were repeated ten times to evaluate different aspects, listed below:

- Four predictive models per-lesion and -patient analysis: Performances of radiomics features extracted from PET and PET/CT, respectively, in assessing the treatment response for each lesion (without considering the patient treatment response) and in assessing the patient treatment response;
- Four models per-patient and -lesion analysis considering the only subset of liver lesions;
- Two models to evaluate the performances of PET and PET/CT radiomics features in discriminating liver metastasis from the rest of the other lesions.

2.3. Diagnostic Performance Evaluation

Sensitivity, specificity, positive predictive value (PPV), accuracy, and receiver operating characteristics (ROC) with 95% confidence intervals (C.I.) and areas under the ROC curve (AUROC; 95% C.I.) were calculated to assess the diagnostic performance on prediction of disease progression (dichotomized evaluation = 1) versus stable disease or partial response or complete response (dichotomized evaluation = 0).

3. Results

Fifty-two patients (mean age 62,28 years ± 11.23) who underwent [^{18}F]FDG PET/CT between November 2008 and December 2018 met the inclusions criteria. The main characteristics are summarized in Table 1. Tumor grading was distributed as follows: G1 in 2/52 (3.85%); G2 in 23/52 (44.23%); G2-3 in 2/52 (3.85%); G3 in 10/52 (19.23%); unknown in 15/52 (28.84%). TNM staging was distributed as follows: Stage I in 4/52 patients (7.69%); Stage II in 9/52 (17.03%); Stage III in 13/52 (25%); Stage IV in 10/52 (19.23%), unknown in 16/52 (30.76%). As first adjuvant therapy, 1 patient (1.92%) was treated by radiotherapy, 49 patients (94.2%) by chemotherapy, and 2 patients (3.85%) by chemotherapy associated with radiotherapy.

Table 1. Patients' main characteristics.

All Patients (n = 52)	
Age (Mean ± SD)	62.28 ± 11.23 y
Sex	
Male	41 (77.35%)
Female	11 (22.65%)
Grading	
G1	2 (3.85%)
G2	23 (44.23%)
G2–G3	2 (3.85%)
G3	10 (19.23%)
Unknown	15 (28.84%)
First Adjuvant Therapy	
Radiotherapy	1 (1.92%)
Chemotherapy	49 (94.2%)
Cht+RT	2 (3.85%)
PET Lesions	
Liver	23 (36.51%)
Lymph nodes	13 (19.05%)
Lungs	8 (12.7%)
Presacral	7 (11.11%)
Peritoneum	4 (6.35%)
Rectum	3 (4.76%)
Spleen	2 (3.17%)
Bones	2 (3.17%)
Thorax	1 (1.59%)
Stages At Diagnosis	
Stage I	4 (7.69%)
Stage II	9 (17.30%)
Stage III	13 (25%)
Stage IV	10 (19.23%)
Unknown	16 (30.76%)

3.1. [^{18}F]FDG PET/CT Findings

At the first [^{18}F]FDG PET/CT scan, 43 patients (82.7%) were PET-positive for a single lesion and 9 (17.3%) for 2 or more lesions. Sites of metastasis were distributed as follows: 23 liver (36.51%), 12 lymph nodes (19.05%), 8 lungs (12.7%), 7 presacral lymph nodes (11.11%), 4 peritoneum (6.35%), 3 rectum (4.76%), 2 spleen (3.17%), 2 bones (3.17%), 1 thorax (1.59%), and 1 anastomosis tissue (1.59%).

3.2. Follow-Up

FU lasted a mean of 22 months (range 13–48 months). We calculated a median progression-free survival (PFS) of 17 months (range 1–105) and a median overall survival of 45 months (range 4–117). At the last FU, 32 (62%) patients showed progression of the disease, 9 (17%) stable disease, and 11 (21%) responded to therapy with a regression of the disease.

3.3. Radiomics Features Analysis

A total of 63 lesions out of 52 patients included in the study were selected. The analysis of the classification model has been divided into three parts, as explained in the "*Radiomics features extraction and Machine-learning features classification*" section, for a total of 10 different radiomics models (Figure 1). In the first case, the prediction disease outcome for each lesion was analyzed (per-lesion analysis) considering the features extracted from PET and PET/CT images, respectively; then, the same analysis was developed of considering each patient (per-patient analysis) considering all the features extracted from the same images for a total of four different radiomics models.

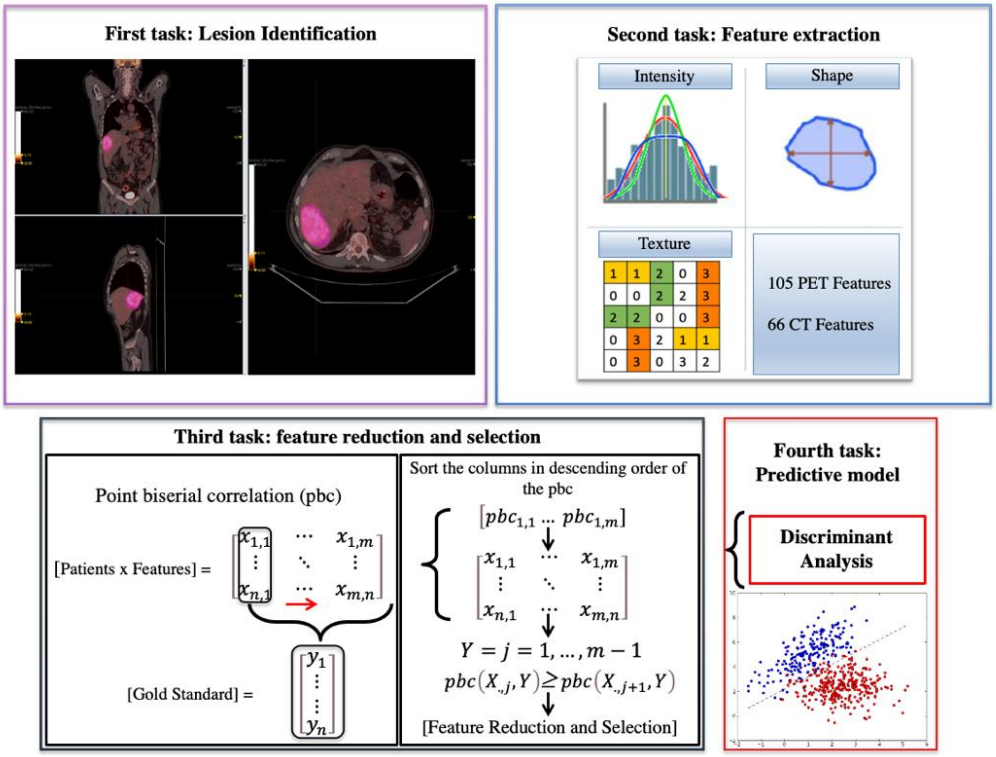

Figure 1. Radiomics flow chart applied in this study.

The results were as follow:

- For lesion analysis, GLRLM-based feature gray-level non-uniformity (GLZLM_GLNU) was selected [15,16] considering the only PET data set obtaining a Sensitivity 90.11%, Specificity 36.78%, Accuracy 66.72%, and AUROC 56.52% for the predictive DA classifier, while three features (GLZLM_ Zone Length Non-Uniformity—GLZLM_ ZLNU, and GLRLM_Short Run High Gray-Level Emphasis—GLRLM_SRHGE—between the CT features and GLZLM_GLNU between the PET features) were selected considering the PET/CT data set with Sensitivity 78.22%, Specificity 51.75%, Accuracy 66.63%, and AUROC 65.22%;
- For patient analysis, three features (GLZLM_ZLNU, GLZLM_High Gray-level Zone -GLZLM_HGZ-, Conventional Radial Intensity Mean Standardized Uptake Value body weight standard deviation squared -CONVENTIONAL_RIM_SUVbwstdev2-) were selected considering the PET-only data set with Sensitivity 32.07%, Specificity 92.11%, Accuracy 73.95% and AUROC 47.97%, and one feature (Conventional Hounsfield Unit Kurtosis -CONVENTIONAL_HUKurtosis-) was selected considering the PET/CT data set with Sensitivity 33.81%, Specificity 83.76%, Accuracy 68.70%, and AUROC 61%.

Figure 2 shows the ROCs for the four implemented models, while Table 2 shows all obtained performances.

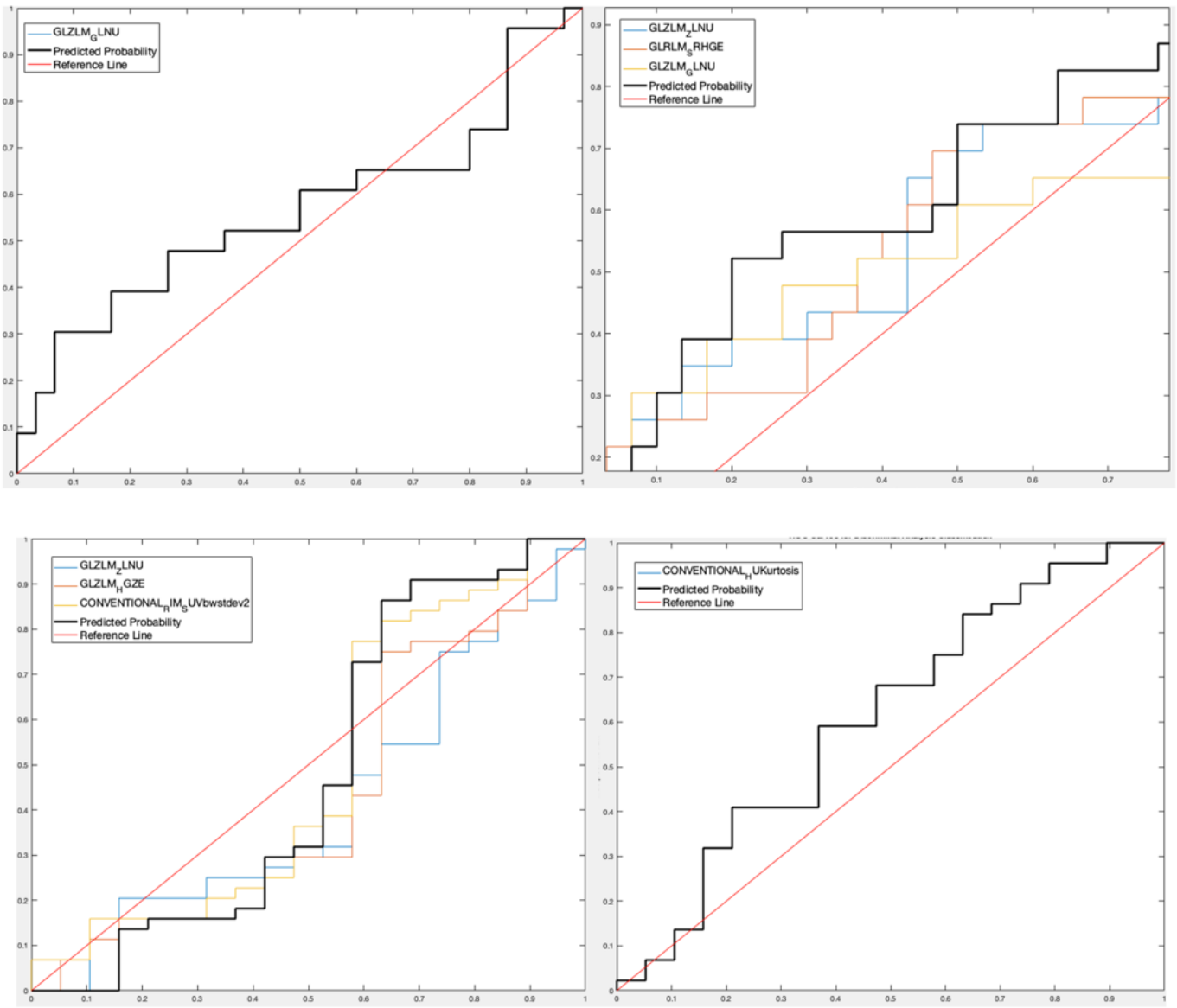

Figure 2. ROCs for the four radiomics models obtained per lesion (first row) and per-patient analyses (second row) for PET-only (first column) and PET/CT images (second column), with an AUROC of 56.52%, 65.22%, 47.97%, and 61%, respectively.

Table 2. Performances of radiomics features in prediction of progression of disease in all lesions, per-patient, and per-lesion analysis.

	Sensitivity	Specificity	Accuracy	AUROC	Features Selected		
PET per-lesion	90.11%	36.78%	66.72%	56.52%	GLZLM_GLNU		
PET/CT per-lesion	78.22%	51.75%	66.63%	65.22%	GLZLM_ZLNU (CT)	GLRLM_SRHGE (CT)	GLZLM_GLNU (PET)
PET per-patient	32.07%	92.11%	73.95%	47.97%	GLZLM_ZLNU	GLZLM_HGZ	CONVENTIONAL_RIM_SUVbwstdev2
PET/CT per-patient	33.81%	83.76%	68.70%	61.00%	CONVENTIONAL_HUKurtosis		

In addition, the study was similarly repeated, focusing only on liver lesions, for a total of two different radiomics models, with the following results:

- For lesion analysis, one PET feature (GLZLM_GLNU) with Sensitivity 70.15%, Specificity 23.48%, Accuracy 54.21%, and AUROC 39.94%, and three PET/CT features (GLZLM_ZLNU, and GLRLM_SRHGE between the CT features and GLZLM_GLNU between the PET features) with Sensitivity 64.39%, Specificity 76.71%, Accuracy 68.69%, and AUROC 55.26%;
- For patient analysis, three PET features (GLZLM_ZLNU, GLZLM_HGZ, CONVENTIONAL_RIM_SUVbwstdev2) with Sensitivity 44.42%, Specificity 84.37%, Accuracy 59.03%, and AUROC 60.11%, and one PET/CT feature (CONVENTIONAL_HUKurtosis) with Sensitivity 33.12%, Specificity 73.74%, Accuracy 47.88%, and AUROC 43.48%.

Figure 3 shows the ROCs for the four implemented models, while Table 3 shows all obtained performances.

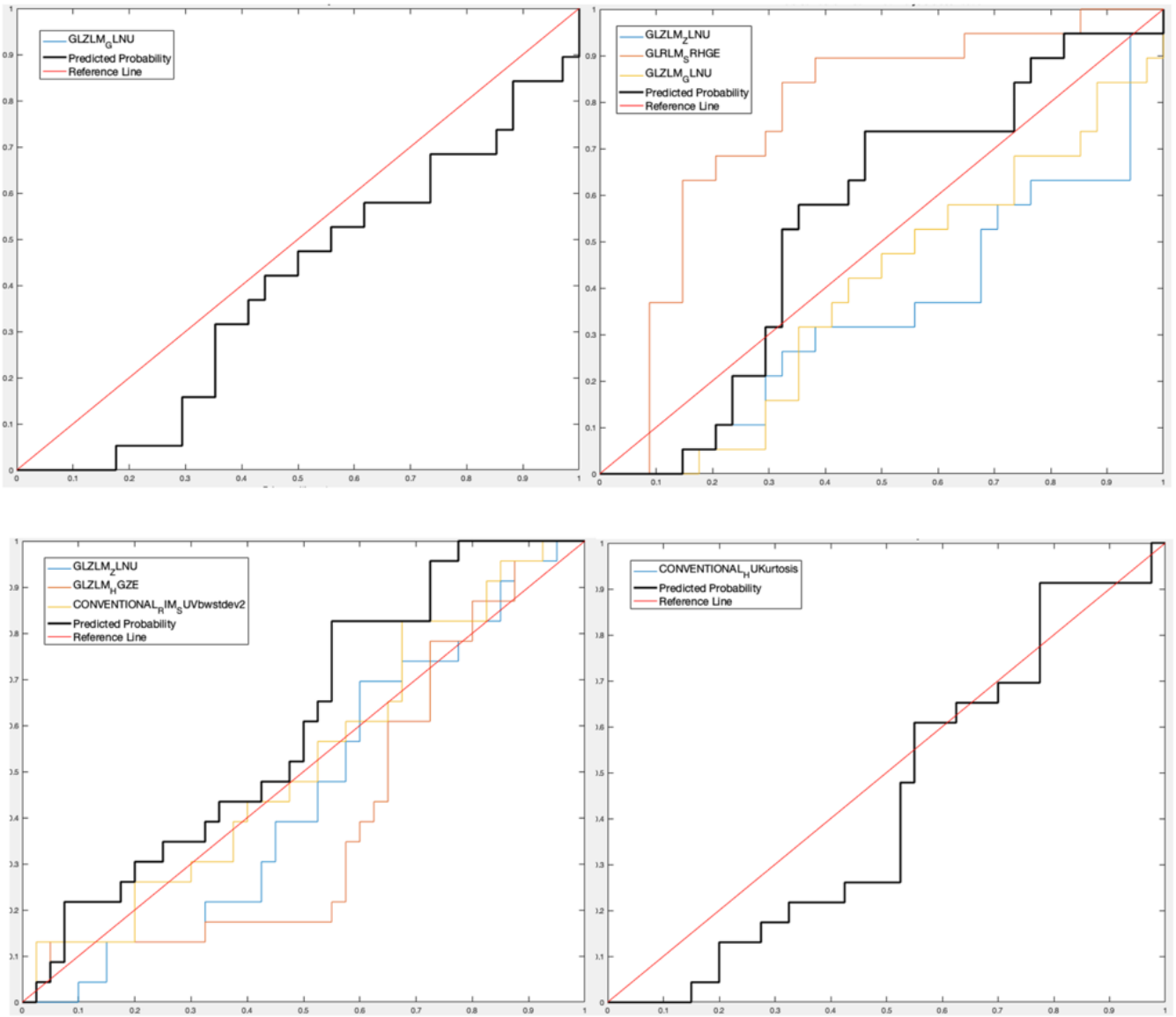

Figure 3. Liver subset: ROCs for the four radiomics models obtained per lesion (first row) and per-patient analyses (second row) for PET (first column) and PET/CT images (second column), with an AUROC of 39.94%, 55.26%, 60.11%, and 43.48%, respectively.

Table 3. Radiomics features performance for liver lesions in prediction of disease progression per-patient and per-lesion analysis.

	Sensitivity	Specificity	Accuracy	AUROC	Features Selected		
PET per-lesion	70.15%	23.48%	54.21%	39.94%	GLZLM_GLNU		
PET/CT per-lesion	64.39%	76.71%	68.69%	55.26%	GLZLM_ZLNU (CT)	GLRLM_SRHGE (CT)	GLZLM_GLNU (PET)
PET per-patient	44.42%	84.37%	59.03%	60.11%	GLZLM_ZLNU	GLZLM_HGZ	CONVENTIONAL_RIM_SUVbwstdev2
PET/CT per-patient	33.12%	73.74%	47.88%	43.48%	CONVENTIONAL_HUKurtosis		

Finally, all lesions were again considered to assess the diagnostic performance of the features in discriminating liver metastasis:

- For PET images, one feature (Discretized SUVbw minimum—DISCRETIZED_SUVbwmin-) was extracted with Sensitivity 73.78%, Specificity 83.02%, Accuracy 76.91%, and AUROC 88.91%;
- For PET/CT images, two features (Discretized histogram energy—DISCRETIZED_HISTO_Energy—between the CT features and DISCRETIZED_SUVbwmin between the PET features) were extracted with Sensitivity 89.46%, Specificity 93.63%, Accuracy 91.02%, and AUROC 95.33%.

Figure 4 shows the ROCs for the two implemented models, while Table 4 shows all obtained performances.

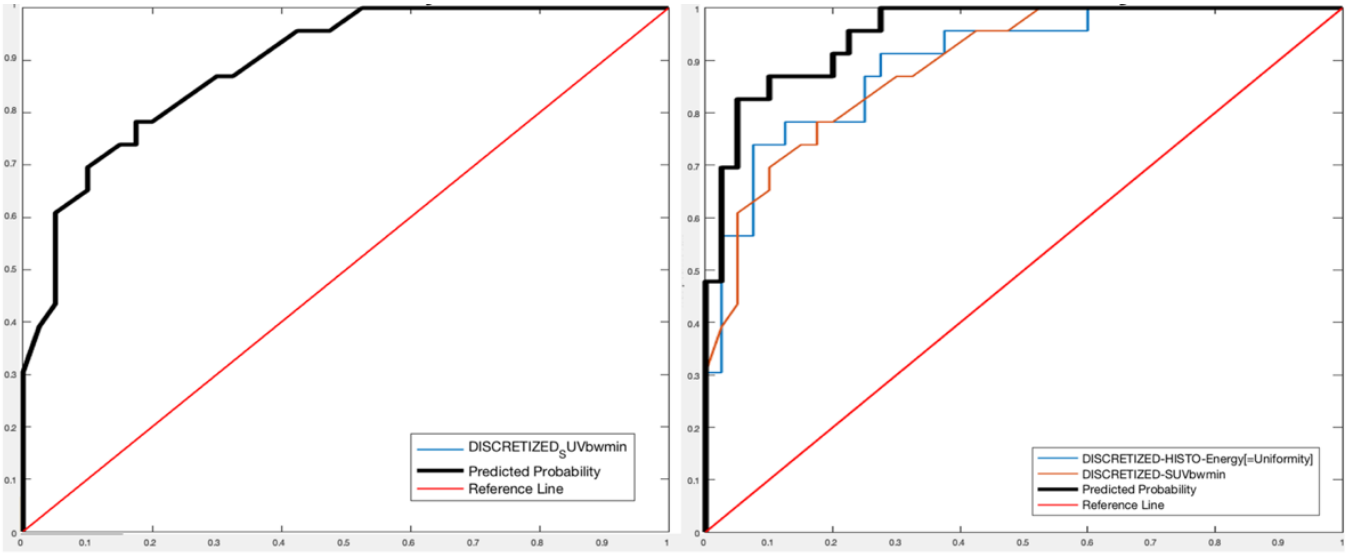

Figure 4. ROCs for the radiomics models implemented for discrimination of liver metastasis using PET and PET/CT images with an AUROC of 88.91% and 95.33%, respectively.

Table 4. Radiomics features performance for liver metastasis discrimination.

	Sensitivity	Specificity	Accuracy	AUROC	Features Selected	
PET liver	73.38%	83.02%	76.91%	88.91%	DISCRETIZED_SUVbwmin	
PET/CT liver	89.46%	93.63%	91.02%	95.33%	DISCRETIZED_HISTO_Energy (CT)	DISCRETIZED_SUVbwmin (PET)

4. Discussion

To the best of our knowledge, the present study is one of the first to explore [^{18}F]FDG PET/CT textural features analysis after first adjuvant therapy to potentially predict disease progression and survival outcome as an indirect predictive parameter of second-line therapy responses in metastatic colon cancer patients, using an innovative mixed descriptive-inferential sequential approach for features reduction and selection, and by using DA as a predictive model [17].

Radiomics literature in CRC is highly heterogeneous, but it holds promise for the prediction of outcomes. Most evidence is available for MRI-based radiomics in rectal cancer [23]. A few studies on textural features derived from [^{18}F]FDG PET images at baseline for locally advanced colorectal cancer and before or after starting any neoadjuvant treatments may enable detailed stratification of prognosis in patients with CRC [24–27].

Our study focused on the potential usefulness to extract PET radiomics features and also low-dose CT radiomic features for a "hybrid" textural PET/CT analysis mimicking the qualitative assessment in the clinical routine evaluation of PET/CT images. The scope of this design study was to confirm the feasibility of our ML methods and to analyze how all the information related to restaging PET/CT imaging after first-line treatments might be able to predict the disease status outcomes after further treatments. Radiomics features were extracted from each lesion (including all the sites of metastasis), divided into three feature subsets: 105 features from PET images, 66 features from CT, and 171 features from both PET and CT. Features were automatically extracted using the well-known IBSI compliant LifeX software to perform a totally objective and reproducible study. Prediction of outcome in patients with CRC is challenging because of the lack of a robust biomarker and heterogeneity between and within tumors to modulate treatment strategies. In this scenario, a study conducted on third-line treatment patients with metastatic colorectal cancer showed that high tumor heterogeneity, volume, and low sphericity on baseline [^{18}F]FDG PET were related to reduced survival [28]. Similarly, textural parameters as the coefficient of variation, kurtosis of the absolute gradient (GrKurtosis), and other features on [^{18}F]FDG PET images have been proposed in other papers as predictive and prognostic factors in the assessment of therapy response and survival outcomes in patients with rectal cancer [29,30].

Our study results, differently from others studies for study design and ML models adopted, demonstrate the potential predictive value of radiomics features derived from an innovative machine learning model adapted by using the disease status at follow-up as the gold standard for the performances analysis. This approach was proposed, as in other studies conducted by our group [31,32], to define the real value of PET/CT as a predictive tool for the stratification of patients with different diseases (prostate and primary brain tumors) that for specific characteristics are more susceptible to have a scarce sensitivity to therapies and a poor disease outcome. For this reason, the apparent sub-optimal results obtained in the present study need to be interpreted with caution because we are not presenting the performance on the identification of disease but the capability of some radiomics features to predict the disease status outcome of the patients with metastatic colon cancer after the standard first adjuvant therapy.

Underlining the results on the PET radiomics analysis in the whole patient group, among per-lesion analysis, the feature selected as the most accurate for the DA classifier was GLZLM_GLNU, while three features (GLZLM_ZLNU and GLRLM_SRHGE between CT features and GLZLM_GLNU between PET features) were selected from PET/CT images obtaining slight enhancement of accuracy when CT analysis was merged with PET performances (AUROC 65.22%).

In per-patient analysis, 3 PET features (GLZLM_ZLNU, GLZLM_HGZ, RIM_SUV bwstdev2), and 1 PET/CT feature (HUKurtosis) were selected by DA classifier (AUROC 61%). Considering these first two analysis groups, three features belonging to the GLZLM class were identified as the most accurate for the DA classifier. The GLZLM, also called gray-level size-zone matrix (GLSZM), is the texture class that provides information on the

size of homogeneous zones for each gray-level. Consequently, it is indirectly linked to the heterogeneity of the lesions, which, reflecting biological characteristics, has a potential value in predicting the progression of the disease [9].

In regard to colorectal liver metastasis, the presence of metastasis in this site is widely considered as one of the unfavorable prognosis parameters. However, commonly employed SUV metrics (SUV_{max}, SUV_{peak}, SUV_{mean}) from [^{18}F]FDG PET images perform relatively poorly in outcome prediction tasks (OS, PFS, EFS). In contrast, the use of liver metastasis number and volumetric measurements of MTV and TLG appears to be capable of providing significant performance [33]. Our radiomics model results, similarly, showed sub-optimal performances in the prediction of disease outcome by defining, at per-lesion analysis, one PET feature (GLZLM_GLNU with AUROC 39.94%) and three PET/CT features (GLZLM_ZLNU and GLRLM_SRHGE between CT features and GLZLM_GLNU between PET features with AUROC 55.26%). Similarly, in liver lesions per-patient analysis, we found 3 PET features (GLZLM_ZLNU, GLZLM_HGZ, RIM_SUVbwstdev2 with AUROC 60.11%) and one PET/CT feature (HUKurtosis with AUROC 43.48%).

Furthermore, to quantify the influence of liver metastasis over all PET/CT findings, one only feature considering PET imaging (i.e., DISCRETIZED_SUVbwmin) and two features considering PET/CT imaging (DISCRETIZED_HISTO_Energy between the CT features and DISCRETIZED_SUVbwmin between the PET features) was able to discriminate liver metastasis from the rest of the other lesions (AUROC = 88.91% and 95.33%, respectively). These results, confirmed after further investigations, may be interpreted as crucial in the diagnostic and prognostic impact of liver lesions in patients affected by metastatic colorectal cancer.

Potential limitations of the study must be considered. First, some intrinsic biases as the well-known sub-optimal accuracy of PET in some conditions due to FDG uptake variability, depending on the histology, size, location (particularly relevant for primary lesion in terms of prognosis: right vs. left colorectal cancer), pH, and possible overestimation of metabolic activity due to associate inflammation, could have affected the results. Furthermore, this is a retrospective single-center study, with a relatively small number of patients and a design study limited by data available. All patients who underwent [^{18}F]FDG PET/CT after the first adjuvant therapy were at different disease stages, treated with different chemotherapy combinations following Italian oncological guidelines (5FU or oral capecitabine in combination with either oxaliplatin or irinotecan in various schedules) and a different number of cycles based on patients clinical conditions. All these variables might affect the patient's outcome. In addition, radiomics features were extracted only from the [^{18}F]FDG-positive tumor to construct the model, and the remaining normal tissue in the image may still contain invisible but useful data. To properly analyze the entire images, 3D deep learning methods will be necessary.

Our study results could benefit from validation in a prospective multi-center study. Nevertheless, our preliminary experience suggests that PET texture analysis is feasible and could carefully be used as an independent indicator for the prognosis of patients with a high risk of disease progression and supporting clinicians for a more accurate selection of patients that may benefit from tailored therapies.

As future research direction of our study, radiomics analyses based on wavelet and Laplacian of Gaussian features will also be considered (e.g., using Pyradiomics) [34]. Furthermore, machine learning investigation could be conducted in the staging preoperative scan, aiming to identify patients with an increased risk of liver metastases susceptible to liver-directed therapies, as previously reported in CT textural analysis by Creasy et al. [35].

5. Conclusions

Our machine learning model on restaging [^{18}F]FDG PET/CT demonstrated to be feasible and potentially useful in the predictive evaluation of disease progression in metastatic colon cancer after first-line therapies. New investigations might propose morpho-

functional-based radiomics algorithms for risk stratification and impact on treatment management in colorectal cancer.

Author Contributions: Conceptualization, P.A.; methodology, P.A., A.S. (Alessandro Stefano) and A.C.; software, A.C.; validation, A.S. (Alessandro Stefano); formal analysis, F.P., C.L. and R.L. (Riccardo Laudicella); investigation, A.C.; resources, A.S. (Alessandro Spataro), G.F., H.L., F.M., V.B. and L.L.G.; writing—original draft preparation, P.A., A.S. (Alessandro Stefano), A.C. and R.L. (Riccardo Laudicella); writing—review and editing, P.A., A.S. (Alessandro Stefano) and A.C.; visualization, A.C.; supervision, I.A.B., T.V.B., S.B., R.L. (Roberto Lagalla), M.M. and G.R. All authors have read and agreed to the published version of the manuscript.

Funding: This research received no external funding.

Institutional Review Board Statement: The study was conducted according to the Declaration of Helsinki principles and good clinical practice guidelines, and written informed consent was obtained by each patient included in the study. For this type of study, ethical approbation was not required in our institution.

Informed Consent Statement: Informed consent was obtained from all subjects involved in the study.

Data Availability Statement: Data are available for bona fide researchers who request it from the authors.

Conflicts of Interest: The authors of this manuscript declare no relationships with any companies whose products or services may be related to the subject matter of the article.

References

1. Sung, H.; Ferlay, J.; Siegel, R.L.; Laversanne, M.; Soerjomataram, I.; Jemal, A.; Bray, F. Global Cancer Statistics 2020: GLOBOCAN Estimates of Incidence and Mortality Worldwide for 36 Cancers in 185 Countries. *CA Cancer J. Clin.* **2021**, *71*, 209–249. [CrossRef]
2. Li, Y.; Eresen, A.; Lu, Y.; Yang, J.; Shangguan, J.; Velichko, Y.; Yaghmai, V.; Zhang, Z. Radiomics signature for the preoperative assessment of stage in advanced colon cancer. *Am. J. Cancer Res.* **2019**, *9*, 1429–1438. [PubMed]
3. Laudicella, R.; Comelli, A.; Stefano, A.; Szostek, M.; Crocè, L.; Vento, A.; Spataro, A.; Comis, A.D.; La Torre, F.; Gaeta, M.; et al. Artificial Neural Networks in Cardiovascular Diseases and its Potential for Clinical Application in Molecular Imaging. *Curr. Radiopharm.* **2020**, *14*, 209–219. [CrossRef] [PubMed]
4. Cook, G.J.; Azad, G.; Owczarczyk, K.; Siddique, M.; Goh, V. Challenges and Promises of PET Radiomics. *Int. J. Radiat. Oncol. Biol. Phys.* **2018**, *102*, 1083–1089. [CrossRef] [PubMed]
5. Liberini, V.; Laudicella, R.; Capozza, M.; Huellner, M.; Burger, I.; Baldari, S.; Terreno, E.; Deandreis, D. The Future of Cancer Diagnosis, Treatment and Surveillance: A Systemic Review on Immunotherapy and Immuno-PET Radiotracers. *Molecules* **2021**, *26*, 2201. [CrossRef]
6. Mayerhoefer, M.E.; Materka, A.; Langs, G.; Häggström, I.; Szczypiński, P.; Gibbs, P.; Cook, G. Introduction to Radiomics. *J. Nucl. Med.* **2020**, *61*, 488–495. [CrossRef]
7. Alongi, P.; Laudicella, R.; Gentile, R.; Scalisi, S.; Stefano, A.; Russo, G.; Emanuele, G.; Domenico, A.; Giancarlo, P.; Sinagra, E.; et al. Potential clinical value of quantitative fluorine-18-fluorodeoxyglucose-PET/computed tomography using a graph-based method analysis in evaluation of incidental lesions of gastrointestinal tract: Correlation with endoscopic and histopathological findings. *Nucl. Med. Commun.* **2019**, *40*, 1060–1065. [CrossRef]
8. Watanabe, A.; Harimoto, N.; Yokobori, T.; Araki, K.; Kubo, N.; Igarashi, T.; Tsukagoshi, M.; Ishii, N.; Yamanaka, T.; Handa, T.; et al. FDG-PET reflects tumor viability on SUV in colorectal cancer liver metastasis. *Int. J. Clin. Oncol.* **2019**, *25*, 322–329. [CrossRef]
9. Chowdhury, R.; Ganeshan, B.; Irshad, S.; Lawler, K.; Eisenblätter, M.; Milewicz, H.; Rodriguez-Justo, M.; Miles, K.; Ellis, P.; Ng, T.; et al. The use of molecular imaging combined with genomic techniques to understand the heterogeneity in cancer metastasis. *Br. J. Radiol.* **2014**, *87*, 20140065. [CrossRef]
10. Chen, S.-W.; Shen, W.-C.; Chen, W.T.-L.; Hsieh, T.-C.; Yen, K.-Y.; Chang, J.-G.; Kao, C.-H. Metabolic Imaging Phenotype Using Radiomics of [^{18}F]FDG PET/CT Associated with Genetic Alterations of Colorectal Cancer. *Mol. Imaging Biol.* **2019**, *21*, 183–190. [CrossRef]
11. Li, J.; Yang, Z.; Xin, B.; Hao, Y.; Wang, L.; Song, S.; Xu, J.; Wang, X. Quantitative Prediction of Microsatellite Instability in Colorectal Cancer with Preoperative PET/CT-Based Radiomics. *Front. Oncol.* **2021**, *11*, 702055. [CrossRef] [PubMed]
12. Boellaard, R.; Delgado-Bolton, R.; Oyen, W.J.G.; Giammarile, F.; Tatsch, K.; Eschner, W.; Verzijlbergen, F.J.; Barrington, S.F.; Pike, L.C.; Weber, W.A.; et al. FDG PET/CT: EANM procedure guidelines for tumour imaging: Version 2. *Eur. J. Nucl. Med. Mol. Imaging* **2015**, *42*, 328–354. [CrossRef] [PubMed]
13. Nioche, C.; Orlhac, F.; Boughdad, S.; Reuzé, S.; Goya-Outi, J.; Robert, C.; Pellot-Barakat, C.; Soussan, M.; Frouin, F.; Buvat, I. LIFEx: A Freeware for Radiomic Feature Calculation in Multimodality Imaging to Ac-celerate Advances in the Characterization of Tumor Heterogeneity. *Cancer Res.* **2018**, *78*, 4786–4789. [CrossRef] [PubMed]

14. Stefano, A.; Leal, A.; Richiusa, S.; Trang, P.; Comelli, A.; Benfante, V.; Cosentino, S.; Sabini, M.G.; Tuttolomondo, A.; Altieri, R.; et al. Robustness of PET Radiomics Features: Impact of Co-Registration with MRI. *Appl. Sci.* **2021**, *11*, 10170. [CrossRef]
15. Comelli, A.; Stefano, A.; Coronnello, C.; Russo, G.; Vernuccio, F.; Cannella, R.; Salvaggio, G.; Lagalla, R.; Barone, S. Radiomics: A New Biomedical Workflow to Create a Predictive Model. In *Annual Conference on Medical Image Understanding and Analysis*; Communications in Computer and Information Science; Springer: Cham, Switzerland, 2020; pp. 280–293, Volume 1248 CCIS, ISBN 9783030527907. [CrossRef]
16. Barone, S.; Cannella, R.; Comelli, A.; Pellegrino, A.; Salvaggio, G.; Stefano, A.; Vernuccio, F. Hybrid descriptive-inferential method for key feature selection in prostate cancer radiomics. *Appl. Stoch. Model. Bus. Ind.* **2021**, *37*, 961–972. [CrossRef]
17. Stefano, A.; Comelli, A.; Bravatà, V.; Barone, S.; Daskalovski, I.; Savoca, G.; Sabini, M.G.; Ippolito, M.; Russo, G. A preliminary PET ra-diomics study of brain metastases using a fully automatic segmentation method. *BMC Bioinform.* **2020**, *21*, 325. [CrossRef]
18. Russo, G.; Stefano, A.; Alongi, P.; Comelli, A.; Catalfamo, B.; Mantarro, C.; Longo, C.; Altieri, R.; Certo, F.; Cosentino, S.; et al. Feasibility on the Use of Radiomics Features of 11[C]-MET PET/CT in Central Nervous System Tumours: Preliminary Results on Potential Grading Discrimination Using a Machine Learning Model. *Curr. Oncol.* **2021**, *28*, 5318–5331. [CrossRef]
19. Comelli, A.; Stefano, A.; Bignardi, S.; Coronnello, C.; Russo, G.; Sabini, M.G.; Ippolito, M.; Yezzi, A. Tissue Classification to Support Local Active Delineation of Brain Tumors. In *Annual Conference on Medical Image UnderStanding and Analysis*; Communications in Computer and Information Science; Springer: Cham, Switzerland, 2020; pp. 3–14, Volume 1065 CCIS, ISBN 9783030393427. [CrossRef]
20. Cuocolo, R.; Comelli, A.; Stefano, A.; Benfante, V.; Dahiya, N.; Stanzione, A.; Castaldo, A.; De Lucia, D.R.; Yezzi, A.; Imbriaco, M. Deep Learning Whole-Gland and Zonal Prostate Segmentation on a Public MRI Dataset. *J. Magn. Reson. Imaging* **2021**, *54*, 452–459. [CrossRef]
21. Comelli, A.; Coronnello, C.; Dahiya, N.; Benfante, V.; Palmucci, S.; Basile, A.; Vancheri, C.; Russo, G.; Yezzi, A.; Stefano, A. Lung Segmentation on High-Resolution Computerized Tomography Images Using Deep Learning: A Preliminary Step for Radiomics Studies. *J. Imaging* **2020**, *6*, 125. [CrossRef]
22. Stefano, A.; Comelli, A. Customized Efficient Neural Network for COVID-19 Infected Region Identification in CT Images. *J. Imaging* **2021**, *7*, 131. [CrossRef]
23. Staal, F.C.; van der Reijd, D.J.; Taghavi, M.; Lambregts, D.M.; Beets-Tan, R.G.; Maas, M. Radiomics for the Prediction of Treatment Outcome and Survival in Patients with Colorectal Cancer: A Systematic Review. *Clin. Color. Cancer* **2020**, *20*, 52–71. [CrossRef] [PubMed]
24. Kang, J.; Lee, J.H.; Lee, H.S.; Cho, E.S.; Park, E.J.; Baik, S.H.; Lee, K.Y.; Park, C.; Yeu, Y.; Clemenceau, J.R.; et al. Radiomics Features of ^{18}F-Fluorodeoxyglucose Positron-Emission Tomography as a Novel Prog-nostic Signature in Colorectal Cancer. *Cancers* **2021**, *13*, 392. [CrossRef] [PubMed]
25. Shen, W.-C.; Chen, S.-W.; Wu, K.-C.; Lee, P.-Y.; Feng, C.-L.; Hsieh, T.-C.; Yen, K.-Y.; Kao, C.-H. Predicting pathological complete response in rectal cancer after chemoradiotherapy with a random forest using ^{18}F-fluorodeoxyglucose positron emission tomography and computed tomography radiomics. *Ann. Transl. Med.* **2020**, *8*, 207. [CrossRef] [PubMed]
26. Lovinfosse, P.; Polus, M.; Van Daele, D.; Martinive, P.; Daenen, F.; Hatt, M.; Visvikis, D.; Koopmansch, B.; Lambert, F.; Coimbra, C.; et al. FDG PET/CT radiomics for predicting the outcome of locally advanced rectal cancer. *Eur. J. Pediatr.* **2018**, *45*, 365–375. [CrossRef]
27. Giannini, V.; Mazzetti, S.; Bertotto, I.; Chiarenza, C.; Cauda, S.; Delmastro, E.; Bracco, C.; Di Dia, A.; Leone, F.; Medico, E.; et al. Predicting locally advanced rectal cancer response to neoadjuvant therapy with ^{18}F-FDG PET and MRI radiomics features. *Eur. J. Pediatr.* **2019**, *46*, 878–888. [CrossRef]
28. Van Helden, E.J.; Vacher, Y.J.L.; van Wieringen, W.N.; van Velden, F.H.P.; Verheul, H.M.W.; Hoekstra, O.S.; Boellaard, R.; Menke-van der Houven van Oordt, C.W. Radiomics analysis of pre-treatment [^{18}F]FDG PET/CT for patients with metastatic colorectal cancer undergoing palliative systemic treatment. *Eur. J. Nucl. Med. Mol. Imaging.* **2018**, *45*, 2307–2317. [CrossRef]
29. Bundschuh, R.A.; Dinges, J.; Neumann, L.; Seyfried, M.; Zsótér, N.; Papp, L.; Rosenberg, R.; Becker, K.; Astner, S.T.; Essler, M.; et al. Textural Parameters of Tumor Heterogeneity in ^{18}F-FDG PET/CT for Therapy Response Assessment and Prognosis in Patients with Locally Advanced Rectal Cancer. *J. Nucl. Med.* **2014**, *55*, 891–897. [CrossRef]
30. Bang, J.-I.; Ha, S.; Kang, S.-B.; Lee, K.-W.; Lee, H.S.; Kim, J.-S.; Oh, H.-K.; Lee, H.-Y.; Kim, S.E. Prediction of neoadjuvant radiation chemotherapy response and survival using pretreatment [^{18}F]FDG PET/CT scans in locally advanced rectal cancer. *Eur. J. Pediatr.* **2015**, *43*, 422–431. [CrossRef]
31. Alongi, P.; Laudicella, R.; Stefano, A.; Caobelli, F.; Comelli, A.; Vento, A.; Sardina, D.; Ganduscio, G.; Toia, P.; Ceci, F.; et al. Choline PET/CT features to predict survival outcome in high risk prostate cancer restaging: A preliminary machine-learning radiomics study. *Q. J. Nucl. Med. Mol. Imaging* **2020**. [CrossRef] [PubMed]
32. Alongi, P.; Stefano, A.; Comelli, A.; Laudicella, R.; Scalisi, S.; Arnone, G.; Barone, S.; Spada, M.; Purpura, P.; Bartolotta, T.V.; et al. Radiomics analysis of 18F-Choline PET/CT in the prediction of disease outcome in high-risk prostate cancer: An explorative study on machine learning feature classification in 94 patients. *Eur. Radiol.* **2021**, *31*, 4595–4605. [CrossRef]
33. Rahmim, A.; Bak-Fredslund, K.P.; Ashrafinia, S.; Lu, L.; Schmidtlein, C.; Subramaniam, R.M.; Morsing, A.; Keiding, S.; Horsager, J.; Munk, O.L. Prognostic modeling for patients with colorectal liver metastases incorporating FDG PET radiomic features. *Eur. J. Radiol.* **2019**, *113*, 101–109. [CrossRef] [PubMed]

34. Jha, A.K.; Mithun, S.; Jaiswar, V.; Sherkhane, U.B.; Purandare, N.C.; Prabhash, K.; Rangarajan, V.; Dekker, A.; Wee, L.; Traverso, A. Repeatability and reproducibility study of radiomic features on a phantom and human cohort. *Sci. Rep.* **2021**, *11*, 2055. [CrossRef] [PubMed]
35. Creasy, J.M.; Cunanan, K.M.; Chakraborty, J.; McAuliffe, J.C.; Chou, J.; Gonen, M.; Ba, V.S.K.; Weiser, M.R.; Balachandran, V.P.; Drebin, J.A.; et al. Differences in Liver Parenchyma are Measurable with CT Radiomics at Initial Colon Resection in Patients that Develop Hepatic Metastases from Stage II/III Colon Cancer. *Ann. Surg. Oncol.* **2020**, *28*, 1982–1989. [CrossRef] [PubMed]